

The effect of deep ocean currents on different OBSs

Carlos Corela¹, Afonso Loureiro¹, José Luis Duarte¹, Luis Matias¹, Tiago Rebelo², Tiago Bartolomeu²

¹Instituto Dom Luiz, Faculdade de Ciências, Universidade de Lisboa, 1749-016 Lisboa, Portugal

²CEIIA, Av. D. Afonso Henriques, 1825, 4450-017 Matosinhos, Portugal

5 *Correspondence to:* Carlos Corela (ccorela@fc.ul.pt)

Abstract. Ocean bottom seismometers (OBS) are usually deployed for seismological investigations but these objectives are impaired by noise resulting from the ocean environment. We split the OBS recorded seismic noise into three bands, short-period, microseisms and long-period, also known as tilt-noise. We show that the first and third bands are controlled by bottom currents but these are not always a function of the tidal forcing. Instead, we suggest that the ocean bottom has a flow regime 10 resulting from two possible contributions, the permanent low-frequency bottom current and the tidal current. The recorded noise displays the balance between these two currents along the full tidal cycle, between neap and spring tides. In the short-period noise band, the ocean current generates harmonic tremors that corrupt the seismic dataset records. We show that, in the investigated cases, the harmonic tremors result from the interaction between the ocean current and mechanical elements of the 15 OBS that are not essential for sea bottom recording and thus have no geological origin. The data from a new Broadband OBS type, designed and built at Instituto Dom Luiz (University of Lisbon)/CEIIA, hiding non-essential components from the current flow, shows how utmost harmonic noise can be eliminated.

1. Introduction

Ocean Bottom seismometers (OBS) are deep-sea instruments that contain a 3-component seismometer and a hydrophone built with the main purpose of monitoring offshore seismicity of tectonically active areas (e.g., Geissler et al., 2010; Silva et al., 2017), contribute to regional and global seismology studies (e.g., Monna et al., 2013; Civiero et al., 2018; Civiero et al., 2019) and image the marine subsurface (e.g., Bowden et al., 2016; Loureiro et al., 2016; Corela et al., 2017). Typically, these instruments are dropped from a ship into the ocean, and free-fall through the water column until they reach the seafloor.

OBS measures ground motions, much like seismic stations on land do. However, deployment conditions on the 25 seafloor are different from those in the continent as the seismometer can be protected from environmental disturbances (e.g., wind, temperature) through installations several meters underground whereas OBS stays on the seafloor exposed to all oceanic physical phenomena. This makes an OBS more than a seismic station, recording in addition to all types of seismic data (of geological, biological or anthropogenic origin), also oceanographic information (currents) as noise data. The noise of oceanic origin significantly impairs the investigation of all other phenomena leading to major challenges and technical difficulties.

30 This noise can be split into three different bands in spectrograms (Figure 1): i) The short-period band from 0.5Hz to 6.5Hz, the “harmonic tremors” discussed and interpreted either as an instrumental cause, a geological cause or both; ii) from 2s to 20s, a well-known geophysical origin that corresponds to the microseisms band and iii) the long-period band from 20s to 60s dominated by the tilt noise, generally attributed to currents tilting the instrument.

One of the challenges of seismic observations in the oceans regards the efficiency of noise reduction generated by 35 oceanic processes (Webb, 1998). Understanding the sources and amplitudes of seismic noise in the oceans is important for improving OBS design in terms of instrumental capabilities and noise mitigation.

On the short-period band (Figure 1), 0.5-40Hz (limited by the sampling rate of 100Hz), local seismic events, and whale vocalization are widely recorded. Long-lasting harmonics tremor signals are commonly observed in spectrograms of OBS data with frequency content overlapping local earthquake signals. In this same band of interest, the resonance of OBS-

40 sediments coupling could be generally observed. Such problems have been described since the beginning of the development of OBS instruments. The first attempt to describe OBS behaviour in terms of current-generated noise was made near Hawaii (Duennebier et al., 1981; Lewis and Tuthill, 1981; Sutton et al., 1981a,b; Trehu and Solomon, 1981; Tuthill et al., 1981; Zelikovitz and Prothero, 1981; Trehu, 1985a,b; Duennebier et al., 1995). Some of these authors show that resonance, related to the Von Kármán vortex shedding off from the various parts of the instrument can occur when near-bottom currents force
45 the water to flow around an OBS. The current-induced noise was investigated using simultaneous recordings of ocean tides, current speed, seismic noise, and transients' tests to study cross-coupling between the vertical and the horizontal components in several instruments available at that period. Trehu (1985a) performed studies concerning the OBS-sediments coupling at the seafloor and concluded that the resonance was within the seismic main frequency band (2 to 15Hz) for most instrument configurations. For OBSs, a large and heavy seismic sensor package, combined with very soft water-saturated sediments, can
50 result in a resonance system within this band. Sutton et al. (1987), suggested that OBS should be designed as small as possible, with the minimum mass conceivable and maximum symmetry towards the vertical axis, to prevent poor signal fidelity caused by the low shear strengths of most ocean sediments.

Similar results were reported by Kovachev et al. (1997), showing oscillation modes specific to the body of an OBS excited by near-bottom currents. These motions affected the seismic sensor, even when the sensor compartment lies several
55 meters away from the noise source. The presence of oscillating frequencies also affects the shape of recorded earthquake signals as they can also cause oscillations of the mechanical components of the station. Kovachev et al. (1997) concluded that the oscillations were caused by the interaction of the OBS components with the near-bottom current flow. However, unlike the von Kármán vortex mechanism, the observed resonant frequency was independent of the current flow speed. They suggested the formation of vortices on the vibrating components of the OBS as responsible for these oscillations. When the
60 vortex shedding frequency (Strouhal frequency) was close to the resonant frequency of the station element, resonant interaction between the current and mechanical station components takes place leading to an effect called a wake or lock-in in literature (e.g., Skop and Griffin, 1975; Griffin, 1985; Sumer and Fredsoe, 1999, Stähler et al., 2018; Essing et al., 2021). Late in the discussion, frequency locking or mode locking is mentioned to define this effect. Webb (1998) also reported that noise can be locally generated by the interaction between seafloor currents and OBS components. Due to the current flow, a radio antenna
65 or other elements such as cables attached to the OBS structure were observed to vibrate as a strummed string. This, in turn, produced harmonic noise with a narrow and energetic peak at frequencies of a few hertz.

Other studies reported harmonic signals in volcanic, nonvolcanic and hydrothermal regions of the world (Pontoise and Hello, 2002; Tolstoy et al., 2002; Díaz et al., 2007; Monigle et al., 2009; Bazin et al., 2010; Franek et al., 2014) associated with gas venting and/or resonance of fluid-filled cracks. These studies concluded that harmonic tremors could result from
70 sustained pressure fluctuations, probably related to stress variations induced by the tidal change of oceanic load. Research campaigns frequently report that harmonic tremors signals are often tidally modulated (Monigle et al., 2009; Franek et al., 2014; Meier and Schlindwein, 2018; Ugalde et al., 2019, Ramakrushana Reddy et al., 2020). Some of these signals coincide with the occurrence of earthquake swarms (Meier and Schlindwein, 2018), although almost identical to hydrodynamically induced tremors on the OBS structure (Stähler et al., 2018). Recent studies (Stähler et al., 2018, Ugalde et al., 2019,
75 Ramakrushana Reddy et al., 2020 and Essing et al., 2021) show that modern OBS designs are also susceptible to substantial hydrodynamic tremor. Stähler et al. (2018) suggest vortex shedding on protuberant objects of the OBS, such as the recovery buoy or the flagpole, as being the general excitation mechanism. Ugalde et al. (2019) observed harmonic tremor in their data set and suggest resonances of the natural frequency of OBS-sediments coupled system as a source driven by water currents modulated by tides. Essing et al. (2021) emphasized that the tremor episodes typically occur twice per day, starting with
80 fundamental frequencies of 0.5-1Hz showing three distinct stages that are characterized by frequency gliding, mode-locking and large spectral amplitudes. These effects were amplified when vortex-shedding frequencies match the resonance frequency of the structure or the head-buoy rope when regarded as a strummed string.

The microseism noise band, 2-20s (Figure 1), is the noise of the ocean wave's origin. The primary microseisms or single-frequency microseism noise (11-20s) is generated in shallow waters where the depth is less than the wavelength of wind-forced gravity waves (Bromirski et al., 2005) and has periods similar to those of the main ocean swell. The secondary microseisms or double-frequency microseism noise (2–10s) is generated by the nonlinear interaction of ocean waves travelling in opposite directions (Longuet-Higgins, 1950).

The long-period noise band, 20-60s (Figure 1), is generally attributed to currents tilting the OBS which causes a redistribution of the gravitational force between the horizontal and vertical components of the seismometer (Sutton and Duennebier, 1987; Webb, 1998; Duennebier and Sutton, 1995; Crawford and Webb, 2000; An et al., 2021). Current-induced tilt-noise is generated by two processes, a displacement term due to the change in the seismometer position, and a rotation term that comes from the change in the gravitational acceleration on the seismometer. At low frequencies, the rotation term dominates, which can be calculated by the gravitational acceleration and the tilt angle (Crawford and Webb, 2000). The rotational term is generally much larger on the horizontal channels than on the vertical, which makes the low-frequency tilt-noise higher on the horizontals than in the vertical (Crawford and Webb, 2000). When the design choices fixed the seismometer to the OBS structure this will increase current-induced long-period tilt-noise because the OBS structure has a larger cross-section than a smaller external seismometer package (Webb, 1998). Stähler et al. (2018) suggested that the high noise levels on OBS records are created not only by bottom currents but also by the specific seismometer used. Another source for the 20-60s noise band is the infragravity waves, which are characterized by small wave height, long wavelength, and long period (30-500s), inducing long-period noise (>30s) on the vertical component of the seismometer and hydrophone and are related with the main ocean swell recorded on the secondary microseisms (Webb, 1998, 2007; Ardhuin et al., 2015; Doran and Laske, 2015).

Several explanations were given to describe the origin of the high noise levels on the short and long-period noise bands. Typically, these signals have little or no influence on the hydrophone sensor and are only seen in the seismometer records. This study uses the vertical and horizontal components of the seismometer to identify and discuss the origin of the recorded signals. It also presents an OBS design that mitigates the harmonic tremors that we consider of instrumental origin and not generated by geological causes.

2. Bottom Currents

In the deep ocean, where OBS are normally deployed, have been considered until the 1980s as a relatively low energy and quiescent depositional environment where deep water masses flow as relatively slow-moving tabular bodies and deposition is episodically interrupted by down-slope gravity-driven processes (Hernández-Molina et al., 2016). However, theoretical and numerical studies suggest that bottom current flow is efficiently generated by: 1) deep tidal (Garrett and Kunze, 2007); and 2) geostrophic motions (Nikurashin and Ferrari, 2010a; Nikurashin and Ferrari, 2010b; Hernández-Molina et al., 2016) flowing over rough small-scale topography.

These deep internal tides (baroclinic) arise when the surface tide (barotropic), generated by the Sun and Moon, forces dense water up and over seafloor topography (MacKinnon et al., 2013). This happens in the same way that tides pull and push water up and down the beach once or twice a day. As water goes back and forth, up and over, it perturbs the normally flat interfaces between density layers, known as isopycnals, and creates internal waves along those surfaces (MacKinnon, 2013). Internal waves with tidal frequencies have been assumed to be a dominant mechanism for turbulent mixing. Some of that energy dissipates locally, producing a pattern of enhanced turbulence over rough topography. The internal tides have horizontal currents that are typically comparable in strength to the barotropic tidal currents of the order of 0.1 ms^{-1} in the deep ocean and 1 ms^{-1} in shallow seas (Garrett and Kunze, 2007).

The tidal signal in the Western Iberian coast consists of the superposition of several harmonics (tidal constituents) dominated by the semi-diurnal tidal components M_2 (sea-level amplitudes between 100 and 180 cm with a periodicity of

12h42m) followed by S_2 (30-50 cm amplitude and periodicity of 12h00m) giving rise to clear spring-neap tidal modulation of 14.8 days, the fortnightly tidal cycle (Almeida et al., 2006; Hernández-Molina et al., 2016). The tidal wave propagates from south to north as a kelvin wave with amplitudes decreasing offshore and a phase speed close to 900km/h (Almeida et al., 2006; Hernández-Molina et al., 2016). Pure kelvin wave dynamics expect tidal currents to change directions periodically with time, 130 describing an elliptical hodograph rotating counterclockwise and parallel to the coast and usually aligned along bathymetry contours in the ocean interior. However, bathymetric irregularities have a large influence on the adjustment of the speed field and are responsible for the amplification of tidal currents, inversion of rotation of the tidal ellipses and its polarization in certain directions (Almeida et al., 2006). Izquierdo et al. (2019), claim the existence of internal tides mostly at Gorringe Bank (GB) and S. Vincent Canyon (SVC) vicinity in full agreement with the location of hotspots for the generation of M_2 reported by 135 Quaresma and Pichon, (2013).

The permanent flow regime around the Atlantic Iberian margin has several water masses flowing at different depths either in the same or in opposite directions, which generate important along-slope sedimentary processes at the seafloor (Hernández-Molina et al., 2011). For the deep ocean, in SW Iberia, two main water masses have been identified for the OBSs. 140 The Lower Deep Water (LDW), composed mainly of Antarctic Bottom Water (AABW; white dashed line in Figure 2) and flowing regionally below 4000 meters depth, mainly across the abyssal plains, and the North Atlantic Deep water (NADW, red dashed line in Figure 2), flowing in various directions between 1400-4000 meters depth. The topography exerts a strong influence on the bottom current speed of these water masses. Oceanic gateways are essential in controlling water-mass exchange between the abyssal plains, and thereby bottom current speed and pathways. The Discovery Gap (DG in Figure 2) 145 is an important gateway for deep water circulation in Tagus Abyssal Plain associated with higher than normal bottom current speeds, reaching 10 cm/sec and in some locations more than 50 cm/sec (Hernández-Molina et al., 2011). Seamounts also represent important obstacles for water mass circulation, and high bottom-current speed can be identified around their flanks. The deep-water currents capable of eroding, transporting and depositing sediments along the seafloor exhibit relatively high speed and play a dominant depositional role in certain areas when interacting with local seafloor irregularities like seamounts, 150 mounds, hills, scarps and ridges (Hernández-Molina et al., 2016).

The turbulent flow regime observed in the OBSs in SW Iberia may have two contributions, the tidal bottom currents and the permanent low-frequency current. Voet et al., 2020, working near a tall submarine ridge in the Pacific Ocean, observed 155 the superposition of two distinct energy sources, the tidal and permanent low-frequency flows, with a combined bottom-current speed of 20 cm/sec in certain periods. Observations showed a stark contrast between conditions at spring and neap tide. The authors concluded that the tide flow speed, in that particular site, during spring tide, was higher than the permanent low-frequency flow. Likewise, through neap tides, a minimum tide flow speed was observed and the permanent low-frequency flow dominated over the oscillatory tide flow (ibid.). They emphasized that during spring or neap tides when tide flow was 160 stronger or weaker than the low-frequency flow speed, the resulting current flow was reduced when interacting as opposed to and increased when in phase (ibid.). These authors concluded that both, tide and low-frequency flows, interact with bottom topography and the energy dissipation at any given time is dictated by the total flow speed (sum of tidal and permanent low-frequency flow).

3. Data and Methods

From September 2007 to August 2008, an ocean bottom seismometer experiment, NEAREST Project (Integrated 165 observations from NEAR shore sourcES of Tsunamis: towards an early warning system) took place offshore of Cape S. Vincent and in the Gulf of Cádiz (Geissler et al., 2010), in the Portuguese and Moroccan exclusive economic zones, on board an Italian Ship, RV *Urania*, where 24 LOBSTER (OBS) from the German instrument pool for amphibian seismology (DEPAS) were

deployed at depths ranging from 1990 to 5100 meters (Figure 2). The FDSN temporary network 9H was assigned during the years 2007 to 2011.

All instruments were recorded continuously at a 100Hz sampling rate on a 3-component GURALP CMG-40TOBS seismometer of 60s corner period (vertical component Z, horizontal component X and Y, see Figure 3 for orientation) and on 170 a hydrophone HTI-04/01-PCA. The LOBSTER (Alfred-Wegener-Institut, Helmholtz-Zentrum für Polar- und Meeresforschung et al., 2017) components are illustrated in Figure 3. The seismometer, hydrophone, data recorder and batteries comprise the acquisition system while the syntactic foam floats and releaser unit are required only for the recovery of instruments from the seafloor. The flag, radio beacon and flashlight are only needed when OBS surfaces to locate the 175 instrument. The head buoy is only used to help retrieve the instrument from the sea surface to the ship. All the elements, that are not required for data recording, will also be present on the seafloor facing the current flow connected to the instrument frame. The head buoy floats 7-10 meters above the OBS with an 18 mm diameter rope tied to the principal OBS mainframe. There are two loops on this rope for retrieval at roughly 3 metres intervals. The sub-horizontal flagpole has a diameter of 21mm and is 1.3 m long. The radio antenna has a diameter of 1.9 mm and is 42 cm long. Both are firmly attached to the OBS 180 frame. The titanium mainframe has a rigid connection to the gimbaled seismometer. According to Stähler et al. (2018), the German pool used the 60s instrument in a version that was modified by Guralp for OBS by reducing power consumption and adding a mechanical gimbal system for automated levelling. The sensor was placed in a titanium casing which caused modifications on the instrument self-noise. The self-noise exceeded the new low-noise model (NLNM; Peterson, 1993) for periods of more than 10s (Tasic and Runovc, 2012) in the vertical component. In this paper, we will only use the horizontal Y component because most OBS did not register the horizontal X component due to technical problems.

185 During this deployment, all the OBS recorded a plethora of signals (e.g. Corela PhD, 2014). This paper will focus on the harmonic tremors (short-period noise band) and tilt noise spectral windows (long-period noise band) triggered by the bottom current flow. In Figure 2 we mark the OBSs that were affected or not by the ocean bottom current flow. Those affected are in yellow and those that were not are in green. However, in this study, we used the 9H OBS01 and 9H OBS03. The influence of deep current flow, tidal and permanent low-frequency, is expected to be more pronounced near rougher topography. 190 9H OBS01 was located at the Tagus Abyssal plain (TAP), deployed at a depth of 5100 meters, within the influence of AABW, and 9H OBS03 in the middle of the D. Henrique basin at a depth of 3932 meters, within the effect of NADW (Figure 2). Despite the focus, we present information regarding harmonic tremors and tilt noise for all the OBSs.

195 In this work, we also evaluate the harmonic tremor and tilt noise signal recorded on the 9H OBS04 near the São Vincente Canyon (Figure 2), at a depth of 1993 meters, under the influence of the NADW. This particular OBS was the only one that showed a different harmonic tremors signal that polluted all spectra from 0.5Hz to 40Hz, showing a large spectral amplitude. Based on this characteristic was decided to deploy a new broadband OBS developed and built in Portugal at Instituto 200 Dom Luiz (IDL)/CEIA within Project DUNE (PTDC/EAM-OCE/28389/2017) in the same surface position of 9H OBS04 to study his behaviour in harsh conditions regarding higher bottom currents speed. The DUNE OBS (Figure 4) was deployed the two data records despite the long-time interval between them.

The purpose of the DUNE OBS was the mitigation the influence of the deep-sea currents on the instrument. The 205 accessories (flag, radio antenna and head buoy) are all inside the outer orange shell during the free-fall and recording period. After releasing the instrument from the anchor at the seafloor, the flag, radio antenna, flash beacon and head buoy are released from the frame and stand outside the outer shell to simplify its recovery at the surface. For the DUNE campaign, the Guralp Aquarius (120s-100Hz) seismometer was firmly connected to the OBS inner structure, as in the LOBSTER OBS. This sensor is a triaxial orthogonal broadband seismometer operational at +/- 90° with a self-noise of -173 dB re(m/s²)²/Hz at 10s in the vertical component. The OBS is a cylinder with a diameter of one meter and a height of 55 cm.

It should be noted that the amplitude of the tilt-noise band (20-60s) and harmonic tremors (0.5-6.5Hz) are used as a proxy to the bottom flow current speed that impacts the OBS structure. No current meter was used in this work. As a proxy to the tidal forcing of the deep ocean currents, we will use Lagos, Sines and Cascais harbour tide table from 10 to 28 September 2007. This period represents one cycle from spring to neap tide and back to the spring tide (Supplementary Table S1). The location of Lagos, Sines and Cascais tide gauges is given in Figure 2. The tidal time is almost identical at the different locations separated by hundreds of kilometres. It should be noted that the tidal range offshore is lower than the tidal range onshore, however, the tidal time is almost identical at the different locations separated by hundreds of kilometres.

215 4. Results

4.1 Deep ocean current regime as inferred from OBS noise

We concentrate the OBS recorded noise analysis on two frequency bands, the short (harmonic tremors) and the long-period (tilt noise) bands, for which we expected to see a strong tidal control if the noise is generated by deep ocean currents modulated by the tides (spring tides) and the permanent low-frequency flow (neap tide).

220 The spectrograms of 9H OBS01 and 9H OBS03, during the new moon spring tide, are seen in Figure 5 for the horizontal components HHY (vertical components HHZ, in Figure S2, supplement). At the spring tide of 11 September 2007, the tide current flow speed, during the flood and ebb tide, should give higher amplitude in spectrograms in the harmonic tremor and tilt-noise band when impacting the OBS structure. The tidal range, which is the high tide amplitude minus the low tide amplitude, is 2.9/2.8/2.8 meters, measured in Lagos/Sines/Cascais tide gauge. The 9H OBS01 located at TAP, reveals a higher 225 current flow speed during the flood tide, reaching a maximum amplitude of -80dB in the tilt-noise band, and a maximum amplitude of -90 dB in the harmonic tremors band. During the ebb tide, the tilt-noise amplitude on the spectrogram decrease to -110 dB and the harmonic tremors are not triggered. The 9H OBS03 shows a different response. During the ebb tide, the resulting current flow speed tilts the seismometer amplitude to -89 dB and the harmonic tremor to -100 dB. During the flood tide, the maximum tilt-noise amplitude decreases to -110 dB and the harmonic tremors are not triggered.

230 During the first quarter moon, the neap tide of 20 September 2007 (Figure 6), the tidal range measured in Lagos/Sines/Cascais was 0.7/0.7/0.7 meters and the tide current flow speed reaches a minimum. For 9H OBS01 the permanent low-frequency flow dominates over the tide oscillatory flow, with a tilt-noise amplitude of -100 dB which increases to -90 dB during the flood tide. The harmonic tremors reach a maximum amplitude of -100 dB during the flood tide. In the same period, 235 9H OBS03, shows a low-frequency flow domination with amplitude between -110 and -100 dB in the tilt-noise band and the harmonic tremors are not visible.

240 After the full moon (26 September 2007) the spring tide has a tidal range of 3.5/3.5/3.6 meters, measured at Lagos/Sines/Cascais (28 September 2007, Figure 7). The tide current flow speed reaches again to a maximum. The 9H OBS01 impact is higher during the flood tide with a maximum amplitude of -80 dB in the tilt-noise band and a maximum amplitude of -89 dB in the harmonic tremors. During the influence of the ebb tide the tilt-noise amplitude decrease to -105dB with no 245 visible harmonic tremor. Similar spectrograms are observed during both spring tides (11 and 28 September 2007). On 9H OBS03, at the D. Henrique basin, the current flow speed is higher during the ebb tide, attains an amplitude of -100 dB in the tilt-noise band and the harmonic tremors are not triggered. See supplementary figures from S2 to S19 to infer the amplitude, vertical and horizontal Y spectrograms in the tilt-noise band and the harmonic tremors from 10 to 28 September 2007. The recorded amplitude on the spectrograms increases, in the long-period (tilt-noise) band, when the laminar flow that impacts the 250 OBS became a turbulent flow due to an increase in the current flow speed. This boundary we called the current flow speed threshold, which is different for the diverse OBS components, like the floating units and the several titanium tubes which compose the OBS structure.

4.2 Harmonic tremor structure

250 Zooming in on the harmonic tremor, as an example, on 11 September it is possible to observe, during the flood tide, that every OBS component that has a resonant frequency inside the short-period noise domain starts to resonate (Figure 8, 9H OBS01 HHZ). That is the case of the resonance of the head buoy rope, flagpole, radio antenna, and the OBS-sediments coupling. The head buoy rope is tied directly to the OBS's titanium tubing mainframe and held taut by the syntactic foam float. The flagpole and radio antenna have a rigid connection with the titanium frame. The seismic sensor, with a gimbal system, has 255 a firm connection to the titanium mainframe and is pressed against the anchor (see Figure 3).

From the spectrogram, which highlights the harmonic tremors, the first emergent resonance is due to the head buoy rope fundamental frequency (R1), afterwards the rope overtones (R2, R3, R4), radio antenna (A) and finally the flagpole (F) eigen-vibrations. Before and after the harmonic tremors (Figure 8, (1) and (6)), the dominant signal is the natural frequency of 260 OBS-sediments coupling resonance (C), between 5.5 and 5.7Hz, observed during the entire recording period of the campaign. This signal is easily detected between the periods of 7h to 9h and from 16h to 19h on the upper spectrogram.

The head buoy rope fundamental frequency (R1) starts to vibrate around 9h05m. The current flow causes the tensioned cable to strum (Stähler et al., 2018). At 9h15m, the head buoy rope overtones (R2, R3, R4) start to emerge at integer multiples of the fundamental frequency. During this period the Von Kármán vortex shedding off the rope is at a frequency lower than the resonance frequency of the rope and is observed in the phenomena of frequency-gliding. At the same time, the 265 radio antenna (A) starts to resonate and a minor frequency-gliding is observed. At 9h40m, four signals from the head buoy rope are visible, during frequency-gliding, with 0.92Hz, 1.84Hz, 2.76Hz, and 3.68Hz, different from the values reported by Stähler et al., (2018), probably due to different rope length, position of intermediate loops, or observed speed current. The OBS-sediments coupling (C) is amplified at this time with a frequency of around 5.7 Hz. The current flow speed at 10h00m initiated a new effect called a wake or lock-in (Skop and Griffin, 1975; Griffin, 1985 and described by Stähler et al., 2018), 270 denominated mode-locking frequency, stable until 14h00m, which is boosted when vortex shedding frequency is equal or close to the resonant frequency of the rope, radio antenna and flagpole. At 10h30m, the flagpole (F) eigen-vibrations begin, without any frequency gliding, and keep the signal until 13h30m. Between (3) 10h50m and (4) 13h10m (Figure 8), for example, it is possible to identify the flagpole signal (F) with 1.45Hz, radio antenna (A) at 6.4Hz and the fundamental and overtones of the head buoy rope (R1 around 1.17Hz, R2 near 2.34Hz, R3 at 3.51Hz and R4 around 4.68Hz). At (5) 15h30m, R1, R2, R3 and 275 R4 have a noticeable decrease in both amplitude and frequency due to the decrease in current flow speed. Around (6) 18h00m the OBS returns to its natural state and the main observed signal is the natural frequency of the OBS-sediments coupling resonance (C). The recorded amplitude on the spectrograms increases, in the short (harmonic tremors), when the laminar flow that impacts the OBS becomes a turbulent flow due to an increase in the current flow speed. This boundary we, also, called the current flow speed threshold, which is different for the different short-period OBS components that resonate.

280 4.3 Noise levels observed on 9H OBS04 and LX OBS01

During the NEAREST campaign in 2007, twenty-four OBS were deployed and analysed. Most of the OBS were 285 deployed in areas where the current flow speed was not enough to trigger the harmonic tremors (Corela PhD, 2014). However, 9H OBS04 (see Figure 2 for location) was deployed in an area where when the current flow speed impacts the OBS structure gives rise to a different OBS response not observed on the other LOBSTER OBS in the short and long-period band noise. The harmonic tremors and tilt noise showed larger spectral amplitude (-60 dB) when compared with 9H OBS01 and 9H OBS03 (maximum spectral amplitude of -83 dB). The mode-locking observed previously is not always present. This response was observed, as an example, most of the day of 14 October 2007 (Figure 9).

The LX OBS01 was deployed at the same surface location as 9H OBS04 to study the response of the OBS in an environment where a strong current flow speed is expected as noted in previous studies. Searching for periods of strong tilt- 290 noise and associated noise in the first short-period domain, for instance, during the 20 September 2021 (Figure 10), the

harmonic tremors were not triggered, because the radio antenna, flagpole and head buoy rope were isolated from vibrations and safely stowed inside the OBS shell (see Figure 5). However, the natural frequency OBS-sediments coupling was observed as expected because the seismometer is connected firmly to the OBS structure. During the strong current flow speed scenario, it seems that the OBS vibrates when impacted by the current flow.

295

5. Discussion

We processed data on all OBS available during the period of this study. In Figure 2, we mark the OBSs that recorded tilt-noise and harmonics tremors due to ocean bottom currents, in yellow, and those that did not in green (see also Figure S20 in the supplements). As expected, bathymetric irregularities have a large responsibility in the adjustment of the speed flow 300 field. We chose the OBSs, 9H OBS01 and 9H OBS03 because they were installed in positions where the bottom current speed effect is patent. In these two spots, the tidal bottom current, as well as, the permanent low-frequency currents, AABW and NADW, are evident.

The AABW, flowing below 4000 meters, needs oceanic gateways to move across the abyssal plains. The Discovery Gap (DG in Figure 2) is an important gateway for deep water circulation in Tagus Abyssal Plain. As seen in Figure 2, AAWB, 305 a white dashed line, near 9H OBS01, 5100 meters depth at TAP, moves from SW to NE. The bottom tidal current, aligned along the bathymetric contour, the flood tide describes a movement from SW to NE and the ebb tide in the contrary direction. The permanent low-frequency AABW current is in phase with the flood tide and the total flow speed is the sum of the two contributions. This flow speed, during the spring tide of 11 September 2011 (new moon, Figure 5, 9H OBS01 HHY), gives -83 dB (maximum amplitude) in the tilt-noise and -90 dB in the harmonic tremors. During the spring tide of 28 September 2007 310 (full moon, Figure 7, 9H OBS01 HHY), -80 dB in the tilt-noise and -87 dB in the harmonic tremors. During the ebb tide, the tidal and the permanent low-frequency AABW currents are in opposing directions, and the total flow speed decreases. The current flow speed in the tilt-noise band decrease to a maximum amplitude of -110 dB and the harmonic tremors' resonances 315 cease their movement. In both spring tides, the behaviour of the 9H OBS01 is identical. During neap tide, 20 September 2007 (first quarter moon, Figure 6, 9H OBS01 HHY), the permanent low-frequency AABW is noticeable all day with a constant recorded amplitude of -100 dB and, during the period of the flood tide, increases to -90 dB. In these two flood tide periods, the little increase in current flow speed is sufficient for the harmonic tremors resonances to appear with a maximum amplitude 320 of -100 dB.

In Figure 11, we show the Probabilistic Power Spectral Densities (PPSD), from 9H OBS01 Guralp CMG-40TOBS, during the neap and spring tides. It's possible to infer the response of the seismometer, during the laminar flow (Figure 12, left 325 side) and during the turbulent flow (Figure 12, right side). During the neap tide, with laminar flow between 12h and 14h, within the ebb tide of 20 September 2007, the response was acceptable between 3-40Hz and exceeded the new low-noise model for periods higher than 1 s. Within the turbulent flow (Figure 12, right side, flood tide, 20 September 2007, between 19h and 21h, 0.7 m tidal range in Sines), as an example, for 30 s, from the laminar to turbulent flow, the tilt-noise band increases from -100 dB to -93 dB (7 dB) and in harmonics tremors band, at 5 Hz, from -125 dB to -102 dB (23 dB). During 11 September 2007 330 (2.7m tidal range in Sines), from laminar to turbulent flow, increased from -120 dB to -87 dB in the tilt-noise band (37 dB) and harmonics tremors band, 5 Hz, from -127 dB to -90 dB (37 dB). On 28 September 2007 (3.5m tidal range in Sines), from laminar to turbulent flow, increased from -110 dB to -82 dB in the tilt-noise band (28 dB) and in the harmonic tremors band from -130 dB to -85 dB (45 dB). The impact of current flow outcomes seismometer higher spectral amplitudes in the short-period band.

335 In the area of the 9H OBS03, D. Henrique basin, the tide bottom current and the permanent low-frequency current, NADW, are the cause of tilt-noise and harmonics tremors. In this particular basin, the tide bottom current still describes an elliptical hodograph in the counterclockwise direction parallel to the coast. The flood tide is from South to North and the ebb tide is in the opposite direction. The permanent low-frequency current, NADW (red dashed line, Figure 2), shows a direction

from NNW to SSE. The permanent low-frequency NADW is almost in phase with the ebb tide and almost opposite to the
335 flood tide. During the spring tide, 11 September 2007 (Figure 5, 9H OBS03 HHY), the maximum amplitude recorded in the tilt-noise occurred only during the two periods of the ebb tide, -90 dB. Only during these ebb tide periods, the current flow speed threshold is attained and the harmonic tremors rise with a maximum amplitude of -100 dB. During the spring tide of 28 September 2007 (Figure 7, 9H OBS03 HHY), surprisingly the maximum amplitude recorded in the tilt-noise band is -100 dB, during the two periods of the ebb tide. Nevertheless, the current flow speed threshold is not attained and the harmonics tremors
340 are not triggered. One possible explanation is a decreased current flow speed in the permanent low-frequency NADW. This explanation is corroborated by the spectrogram recorded during the neap tide of 20 September (Figure 6, 9H OBS03 HHY) where we see an intermittent flow of the permanent low-frequency NADW current. Consulting the supplement figures, from S2 to S19, is noticeable a speed decrease of permanent low-frequency NADW current flow between 13 and 14 of September 2007 showing two ebb tides and two flood tides. After the 23 of September 2007, the permanent low-frequency NADW current
345 flow increases the speed, in phase again with the ebb tide, however, the total flow speed is less than the current flow speed threshold necessary to initiate the harmonics tremors. During this period, from 11 to 28 September 2007, the permanent low-frequency flow observed in TAP, the AABW current, shows a strong and persistent direction. In contrast, the NADW current is intermittent and has a lower speed flow when compared to the AABW.

We show that the ocean bottom flow, as inferred from the tilt noise, is not an exclusive function of the tidal forcing.
350 Instead, it is shown that the ocean bottom has a flow regime that may have two contributions, the permanent low-frequency current and the tidal current, as mentioned in Voet et al., (2020). The recorded tilt-noise displays the balance between these two currents along the full tidal cycle, between neap and spring tides. From these current flows, it is possible to highlight that the most relevant parameter to the OBS noise recorded is the resulting current flow speed due to both currents or just one of them. In Figure 1, during the neap tide of 19 October 2007, with a tidal range of 0.8 m (measured in Sines), it was possible to
355 observe harmonic tremors features for as long as 24 hours in 9H OBS01. The permanent low-frequency flow was the trigger of the resonance state, but a tidal modulation can still be inferred.

Highlighting the harmonic tremor spectral band, the 9H OBS01 components that have a resonant frequency inside the short-period noise domain, start to resonate during the flood tide. When the current flow speed threshold is reached and exceeded, and when we observed the frequency mode-locking, the vortex shedding frequency is equal to or close to the
360 resonant frequency of the several components of the OBS. This allows us to infer the current flow speed, in this particular location, observed in harmonics tremors. For example, in Figure 8 (4), at 13h10m of 11 September 2007, the observed resonance frequency of the radio antenna is 6.4 Hz and for the flagpole is 1.45 Hz. The shedding frequency is proportional to the Strouhal number, which for this OBS design is 0.21, and to the current flow speed, in cm/sec, and inversely proportional to the diameter of the OBS component (see e.g. Stähler et al., 2018). One of the first components to enter a resonant state is
365 the radio antenna (diameter of 0.19 cm) which only needs a current flow speed of 5.3 to 5.5 cm/sec to reach the frequency mode-locking. For the flagpole, with a diameter of 2.1 cm, it is necessary the current flow speed to be equal to 15 cm/sec. Applying this reasoning to the spectrum of Figure 8, we infer that between 10h10m and 10h30m, the current flow speed is limited to the range of 5 to 15 cm/sec, between 10h30m and 13h30m at least equal or higher than 15 cm/sec, between 13h30m and 14h10m to the range of 15 to 5 cm/sec and between 14h20m to 15h40m below 5 cm/sec. The maximum harmonic tremor
370 spectral amplitude observed in 9H OBS01 was -85 dB (Figure 11). From Figure 12, 9H OBS04, with a maximum harmonic tremor spectral amplitude of -63 dB, one possible conclusion is that the current flow speed can reach 50 cm/sec or more as proposed by Molina et al., (2011).

Due to the large spectral amplitude detected near São Vincent Canyon, owing to the high current flow speed observed in this region, we showed the noise levels of 9H OBS04 and LX OBS01 (Figure 12). Two windows, one with laminar flow
375 and one with turbulent flow, as identified in Figures 9 and 10, were chosen to illustrate the seismometer response when impacted by the current flow. For 9H OBS04, an increase of the spectral amplitude of 47 dB at the tilt noise band (30 sec) was

observed an increase of 56 dB in the short-period band (5 Hz). For the LX OBS01, an increase of 23 dB at the tilt noise band (30 sec) we observed an increase of 23 dB in the short-period band (one spectral line of 3.8 Hz which is the natural frequency of the OBS-sediment coupling resonance). When both stations were impacted by laminar flow (Figure 13), the natural response of the seismometers at the sea bottom was recorded. The GURALP CMG-40T has a normal response between 10s-40Hz and exceeds the new low-noise model for periods above 10s. The GURALP Aquarius show $-160 \text{ dB re(m/s}^2\text{)}^2/\text{Hz}$ between 15 and 20s.

This new design, DUNE OBS, however, is still highly exposed to the current flow. Later iterations are aimed, at the long-period noise band, since the tilt noise still needs to be mitigated. Research into solving this problem is already in progress and further work needs to be carried out to establish improvements in OBS design. Future work should focus on changing the seismic sensor position and disconnection from the OBS structure in a smaller package. This action should shift the natural frequency of the OBS-sediments coupling resonance to above the seismologically interested frequency band and should mitigate the tilt noise. Similar design changes could also improve the signal of the LOBSTER OBS.

This study finds that the harmonic tremors and the tilt-noise signal are independent of the current direction relative to the OBSs in both designs. The features are in all seismometer components (Figure S21 in supplements). However, the difference in the spectral amplitude of the signal, on the horizontal components, could give some insight into the path of the current flow field.

6. Conclusions

Analysing seismic data recorded by OBS in the SW Iberia we showed that both the short-period (0.5Hz-6.5Hz) and long-period (20-60s) noise bands have an environmental origin of deep ocean currents. However, each site is unique in terms of depth, currents and topography. In this work, we show that the ocean bottom flow, as inferred from the tilt noise, is not always dominated by the tidal forcing, but rather that the ocean bottom has a flow regime that may have two independent contributions, the permanent low-frequency current and the tidal current. The recorded noise displays the balance between these two currents along the full tidal cycle, between neap and spring tides and depends on the direction of each flow and the final combined current flow speed.

In the short-period noise domain, we investigated in detail the harmonic tremor band (0.5Hz-6.5Hz) and showed that all the mechanical elements of the OBS that are not essential for recording at sea bottom do resonate when the current speed reaches some threshold. Noise is shown on spectrograms by nearly constant frequency bands and by broadband spectral lines. These findings support the interpretation that the strongest harmonic tremors are the result of the strumming of the head-buoy rope on the LOBSTER design (Stähler et al., 2018; Essing et al., 2021) and confirmed that the radio antenna, flagpole, and the natural frequency of OBS-sediment coupling resonance are also excited by the current flow speed when the laminar flow became turbulent in each component. The head buoy rope's fundamental frequency and respective overtones exhibit frequency-gliding. These characteristics are reported in different studies, however, the strumming rope frequencies reported in this study are different from those reported previously (e.g. Stähler et al., 2018; Essing et al., 2021). The radio antenna also exhibits it, but with a smaller amplitude and the flagpole has no visible frequency-gliding. When the frequency of vortex shedding is near or identical to the resonance frequency of the different components we observe the mode-locking frequency, which gives some insight into the minimum current flow speed threshold that causes that disturbance.

Our study provides evidence for another noise regime, without clear mode-locking frequency when a very strong current flow triggers the several resonance components of the OBS. In 9H OBS04 the observed harmonic tremor starts with frequency gliding but the mode-locking frequency state is attained only on several occasions. The observed harmonic tremor increases the spectral amplitude and enlarged the number of overtones.

References

Alfred-Wegener-Institut, Helmholtz-Zentrum fur Polar- und Meeresforschung.: DEPAS (Deutscher Gerate-Pool fur amphibische Seismologie): German Instrument Pool for Amphibian Seismology, *Journal of largescale research facilities*, 3, 420 A122, <https://doi.org/10.17815/jlsrf-3-165>, 2017.

Almeida, M. M., Dubert, J.: The structure of tides in the Western Iberia region, *Continental Shelf Research* 26, 385-400, <https://doi.org/10.1016/j.csr.2005.11.011>, 2006.

425 An, C., Cai, C., Zhou, L., Yang, T.: Characteristics of low-frequency horizontal noise of ocean-Bottom Seismic data, *Seismology Research Letters*, 93(1), 257-267, <https://doi.org/10.1785/0220200349>, 2022.

Ardhuin, F., Gualtieri, L., and Stutzmann E.: How ocean waves rock the Earth: Two mechanisms explain microseisms with periods 3 to 300s, *Geophys. Res. Lett.* 42, no. 3, 765–772, <https://doi.org/10.1002/2014GL062782>, 2015.

430 Bazin, S., Feuillet, N., Duclos, C., Crawford, W., Nercessian, A., Bengoubou-Valérius, M., Beauducel, F. and Singh, S. C.: The 2004–2005 Les Saintes (French West Indies) seismic aftershock sequence observed with ocean bottom seismometers, *Tectonophysics* 489, 91–103, <https://doi.org/10.1016/j.tecto.2010.04.005>, 2010.

435 Bowden, D. C., Kohler, M.D., Tsai, V. S. and Weeraratne, D. S.: Offshore Southern California lithospheric velocity structure from noise cross-correlation functions, *J. Geophys. Res. Solid Earth*, 121, <https://doi.org/10.1002/2016JB012919>, 2016.

Bromirski, P. D., Duennebier, F. K., and Stephen, R. A.: Midocean microseisms. *Geochem. Geophys. Geosys.* 6, no. 4, <https://doi.org/10.1029/2004GC000768>, 2005.

440 Civiero, C., Strak, V., Custódio, S., Silveira, G., Rawlinson, N., Arroucau, P., Corela, C.: A common deep source for upper-mantle upwellings below the Ibero-western Maghreb region from teleseismic P-wave travel-time tomography, *Journal of Geophysical Research: Solid Earth*, 124, 1781-1801, <https://doi.org/10.1029/2018JB016531>, 2018.

445 Civiero, C., Custódio, S., Rawlinson, N., Strak, V., Silveira, G., Arroucau, P., Corela, C.: Thermal nature of mantle upwellings below the Ibero-western Maghreb region inferred from teleseismic tomography, *Earth and Planetary Science Letters*, 499, 157-172, <https://doi.org/10.1016/j.epsl.2018.07.024>, 2019.

Corela, C.: Ocean bottom seismic noise: applications for the crust knowledge, interaction ocean-atmosphere and instrumental behavior. PhD thesis – Science Faculty of Lisbon University, <http://hdl.handle.net/10451/15805>, 2014.

450 Corela, C, Silveira, G., Matias, L., Schimmel, M. and Geissler, W.: Ambient seismic noise tomography of SW Iberia integrating seafloor and land-based data, *Tectonophysics*, 700-701, 131-149, <https://doi.org/10.1016/j.tecto.2017.02.012>, 2017.

455 Crawford, W. C., Webb, S. C.: Identifying and removing tilt noise from low-frequency(<0.1Hz) seafloor vertical seismic data, *Bulletin of the Seismological Society of America*, 90(4), 952-963, <https://doi.org/10.1785/0119990121>, 2000.

Díaz, J., Gallart, J., and Gaspà, O.: Atypical seismic signals at the Galicia Margin, North Atlantic Ocean, related to the
460 resonance of subsurface fluid-filled cracks, *Tectonophysics* 433, 1–13, <https://doi.org/10.1016/j.tecto.2007.01.004>, 2007.

Doran, A. K., and Laske, G.: Infragravity waves and horizontal seafloor compliance, *J. Geophys. Res.* 121, no. 1, 260–278,
<https://doi.org/10.1002/2015jB012511>, 2015.

Duennbier, F. K., Blackinton, J. G., and Sutton, G.: Current-Generated Noise Recorded on Ocean Bottom Seismometers,
465 *Marine Geophys. Res.* 5, 109–115, <https://doi.org/10.1007/BF00310316>, 1981.

Duennbier, F. K., and Sutton, G. H.: Fidelity of ocean bottom seismometers, *Mar. Geophys. Res.*, 17(6), 535–555,
<https://doi.org/10.1007/BF01204343>, 1995.

470 Essing, D., Schlindwein, V., Schmidt-Aursch, M. C., Hadzioannou, C. and Stähler, S. C.: Characteristics of Current-Induced Harmonic Tremor Signals in Ocean-Bottom Seismometer Records, *Seismol. Res. Lett.* 92(5), 3100–3112,
<https://doi.org/10.1785/0220200397>, 2021.

Franek, P., Mienert, J., Buenz, B., and Géli, L.: Character of seismic motion at a location of a gas hydrate bearing mud volcano
475 on the SW Barents Sea margin, *J. Geophys. Res.* 119, 6159–6177, <https://doi.org/10.1002/2014JB010990>, 2014.

Garrett, C., and Kunze, E.: Internal Tide Generation in the Deep Ocean, *Ann. Rev. Fluid Mech.*, 39, 57–87,
<https://doi.org/10.1146/annurev.fluid.39.050905.110227>, 2007.

480 Geissler, W.H., Matias, L., Stich, D., Carrilho, F., Jokat, W., Monna, S., IbenBrahim, A., Mancilla, F., Gutscher, M.-A., Sallarès, V., Zitellini, N.: Focal mechanisms for sub–crustal earthquakes in the Gulf of Cadiz from a dense OBS deployment, *Geophys. Res. Lett.* 37, L18309, <https://doi.org/10.1029/2010GL044289>, 2010.

Griffin, O. M.: Vortex-induced vibrations of marine cables and structures, Technical Report, Naval Research Lab, Washington,
485 D. C., available at <http://www.dtic.mil/docs/citations/ADA157481>, 1985.

Hernandez-Molina, F. J., Serra, N., Stow, D. A. V., Llave, E., Ercilla, G. & van Rooij, D.: Along-slope oceanographic processes and sedimentary products around the Iberian margin, *Geo-Marine Letters* 31, 5–6, p. 315–341 27 p,
<https://doi.org/10.1007/s00367-011-0242-2>, 2011.

490 Hernández-Molina, F. J., Wåhlin, A., Bruno, M., Ercilla, G., Llave, E., Serra, N., Rosón, G., Puig, P., Rebesco, M., Van Rooij, D., Roque, D., González-Pola, C., Sánchez, F., Gómez, M., Preu, B., Schwenk, T., Hanebuth, T. J. J., Sánchez Leal, R. F., García-Lafuente, J., Brackenridge, R. E. & 3 others: Oceanographic processes and morphosedimentary products along the Iberian Margins: A new multidisciplinary approach, *Marine Geology* 378, 127–156,
<https://doi.org/10.1016/j.margeo.2015.12.008>, 2016.

495 Izquierdo, A., Mikolajewicz, U.: The role of tides in the spreading of Mediterranean Outflow waters along the southwestern Iberian margin, *Ocean Modelling* 133, 27–43, <https://doi.org/10.1016/j.ocemod.2018.08.003>, 2019.

500 Kovachev, S. A., Demidova, T. A., and Son'kin, A. V.: Properties of noise registered by Pop-Up Ocean Bottom Seismographs, Journal of Atmospheric and Oceanic Technology, 883-888, [https://doi.org/10.1175/1520-0426\(1997\)014<0883:PONRBP>2.0.CO;2](https://doi.org/10.1175/1520-0426(1997)014<0883:PONRBP>2.0.CO;2), 1997.

Krischer, L., Megies, T., Barsch, R., Beyreuther, M., Lecocq, T., Caudron, C., and Wassermann, J.: ObsPy: a bridge for seismology into the scientific Python ecosystem, Computational Science & Discovery, 8 (1), 014003. <http://stacks.iop.org/1749-4699/8/i=1/a=014003>, 2015.

505

Lewis, B. and Tuthill, J.: Instrumental Waveform Distortion on Ocean Bottom Seismometers, Marine Geophys. Res. 5, 79-86, <https://doi.org/10.1007/BF00310313>, 1981.

510

Longuet-Higgins, M. S.: A theory of the origin of microseisms, Phil. Trans. Roy. Soc. Lond. A 243, no. 857, 1-35, <https://doi.org/10.1098/rsta.1959.0012>, 1950.

Loureiro, A., Afilhado, A., Matias, L., Moulin, M., Aslanian, D.: Monte Carlo approach to assess the uncertainty of wide-angle layered models: Application to the Santos Basin, Brazil, Tectonophysics 683, 286-307, <https://doi.org/10.1016/j.tecto.2016.05.040>, 2016.

515

MacKinnon, J.: Mountain waves in the deep ocean, *Nature*, 501, 320-321, <https://doi.org/10.1038/501321a>, 2013.

Meier, M., and Schlindwein, V.: First in situ seismic record of spreading events at the ultraslow spreading Southwest Indian ridge, Geophys. Res. Lett. 45, 10,360-10,368, <https://doi.org/10.1029/2018gl079928>, 2018.

520

Monigle, P. W., Bohnenstiehl, D. R., Tolstoy, M., and Waldhauser, F.: Seismic tremor at the 9_500N East Pacific Rise eruption site, Geochem. Geophys. Geosys. 10, <https://doi.org/10.1029/2009GC002561>, 2009.

525

Monna, S., Argnani, A., Cimini, G. B., Frugoni, F., Montuori, C.: Constrains on the geodynamics evolution of the Africa-Iberia plate margin across the Gibraltar Strait from seismic tomography, Geoscience Frontiers, <https://doi.org/10.1016/j.gsf.2014.02.003>, 2014.

Nikurashin, M., and Ferrari, R.: Radiation and dissipation of internal waves generated by geostrophic flows impinging on small-scale topography: Theory, J. Phys. Oceanogr., 40, 1055-1074, <https://doi.org/10.1175/2009JPO4199.1>, 2010a.

530

Nikurashin, M., and Ferrari, R.: Radiation and dissipation of internal waves generated by geostrophic flows impinging on small-scale topography: Application to the Southern Ocean, J. Phys. Oceanogr., 40, 2025-2042, <https://doi.org/10.1175/2010JPO4315.1>, 2010b.

535

Peterson, J.: Observations and Modeling of Seismic Background Noise. U.S.G.S, Open File Report, 93-322, 95 p, 1993.

Pontoise, B., and Hello, Y.: Monochromatic infra-sound waves recorded offshore Ecuador: Possible evidence of methane release, Terra Nova 14, 425-435, <https://doi.org/10.1046/j.1365-3121.2002.00437.x>, 2002.

540 Quaresma, L.S., Pichon, A.: Modelling the barotropic tide along the west-Iberian margin. *J. Mar. Syst.* 109-110, S3–S25, <https://doi.org/10.1016/j.jmarsys.2011.09.016>, 2013.

Ramakrushana Reddy, Dewangan, T. P., Arya, L., Singha, P. and Kamesh Raju, R. A.: Tidal triggering of the harmonic noise in ocean-bottom seismometers, *Seismol. Res. Lett.* 91, 803–813, <https://doi.org/10.1785/0220190080>, 2020.

545

Silva, S., Terrinha, P., Matias, L., Duarte, J. C., Roque, C., Ranero, C. R., Geissler, W. and Zitellini, N.: Micro-seismicity in the Gulf of Cadiz: Is there a link between micro-seismicity, high magnitude earthquakes and active faults?, *Tectonophysics*, 717, 226-241, <https://doi.org/10.1016/j.tecto.2017.07.026>, 2017.

550

Stähler, S. C., Schmidt-Aursch, M. C., Hein, G., and Mars, R.: A self-noise model for the German DEPAS OBS pool. *Seismol. Res. Lett.* 89, 1838–1845, <https://doi.org/10.1785/0220180056>, 2018.

Skop, R. A., and Griffin, O. M.: On a theory for the vortex-excited oscillations of flexible cylindrical structures, *J. Sound Vib.* 41, no. 3, 263–274, [https://doi.org/10.1016/S0022-460X\(75\)80173-8](https://doi.org/10.1016/S0022-460X(75)80173-8), 1975.

555

Sumer, B. M., and Fredsøe, J.: *Hydrodynamics around Cylindrical Structures*, P. Liu (Editor), Vol. 12, Advanced Series on Ocean Engineering, World Scientific, Singapore, <https://doi.org/10.1142/3316>, 1999.

560

Sutton, G. H., Duennbier, F. K., and Iwatake, B.: Coupling of Ocean Bottom Seismometers to Soft Bottom, *Marine Geophys. Res.* 5, 35–51, <https://doi.org/10.1007/BF00310310>, 1981a.

Sutton, G. H., Duennbier, F. K., Iwatake, B., Tuthill, J., Lewis, B., and Ewing, J.: An Overview and General Results of the Lopez Island OBS Experiment, *Marine Geophys. Res.* 5, 3–34, <https://doi.org/10.1007/bf00310309>, 1981b.

565

Sutton, G. H., and Duennbier, F. K.: Optimum design of ocean bottom seismometers, *Mar. Geophys. Res.* 9, no. 1, 47–65, <https://doi.org/10.1007/BF00338250>, 1987.

Tasić, I., Runovc, F.: Seismometer self-noise estimation using a single reference instrument, *J. Seismol.* 16, no. 2, 183–194, <https://doi.org/10.1007/s10950-011-9257-4>, 2012.

570

Trehu, A. M. and Solomon, S. C.: Coupling parameters of the MIT OBS at two nearshore sites, *Marine Geophys. Res.* 5, 69–78, <https://doi.org/10.1007/BF00310312>, 1981.

575

Trehu, A. M.: Coupling of Ocean Bottom Seismometers to Sediment: Results of Tests with the U.S. Geological Survey Ocean Bottom Seismometer, *Bull. Seism. Soc. Am.* 75, 271–289, 1985a.

Trehu, A. M.: A Note on the Effect of Bottom Currents on an Ocean Bottom Seismometer, *Bull. Seism. Soc. Am.* 75, 1195–1204, 1985b.

580

Tolstoy, M., Vernon, F. L., Orcutt, J. A. and Wyatt, F. K.: Breathing of the seafloor: Tidal correlations of seismicity at Axial volcano, *Geology* 30, 503–506, [https://doi.org/10.1130/0091-7613\(2002\)030<0503:BOTSTC>2.0.CO;2](https://doi.org/10.1130/0091-7613(2002)030<0503:BOTSTC>2.0.CO;2), 2002.

Tulhill, J. D., Lewis, B. T. R., Garmany, J. D.: Stoneley waves, Lopez island noise, and deep sea noise from 1 to 5Hz, *Marine Geophysical Researches* 5, 95-108, <https://doi.org/10.1007/BF00310315>, 1981

585

Ugalde, A., Gaite, B., Ruiz, M., Villaseñor, A. and Ranero, C. R.: Seismicity and noise recorded by passive seismic monitoring of drilling operations offshore the Eastern Canary Islands, *Seismol. Res. Lett.* 90, 1565–1576, <https://doi.org/10.1785/0220180353>, 2019.

590 Voet, G. Alford, M. H., and MacKinnon, J.: Topographic form drag on tides and low-frequency flow: Observations of nonlinear Lee Waves over a tall submarine ridge near Palau, *Journal of Physical Oceanography*, 50, 1489-1507, <https://doi.org/10.1175/JPO-D-19-0257.1>, 2020.

595 Webb, S.C.: Broadband seismology and noise under the ocean, *Rew.Geophys.*, 36 1, 105–142, <https://doi.org/10.1029/97RG02287>, 1998.

Webb, S. C.: The Earth’s “hum” is driven by ocean waves over the continental shelves, *Nature* 445, no. 7129, 754–756, <https://doi.org/10.1038/nature05536>, 2007.

600 Wessel, P., Smith, W. H. F., Scharroo, R., Luis, J. F., and Wobbe, F.: Generic Mapping Tools: Improved version released, *Eos Trans. AGU* 94, 409–410, <https://doi.org/10.1002/2013EO450001>, 2013.

Zelikovitz, S. J. and Prothero, W. A.: The vertical response of an ocean bottom seismometer: analysis of the Lopez Island vertical transient tests, *Marine Geophys. Res.* 5, 53-67, <https://doi.org/10.1007/BF00310311>, 1981.

605 Competing interests

The authors declare that they have no conflict of interest.

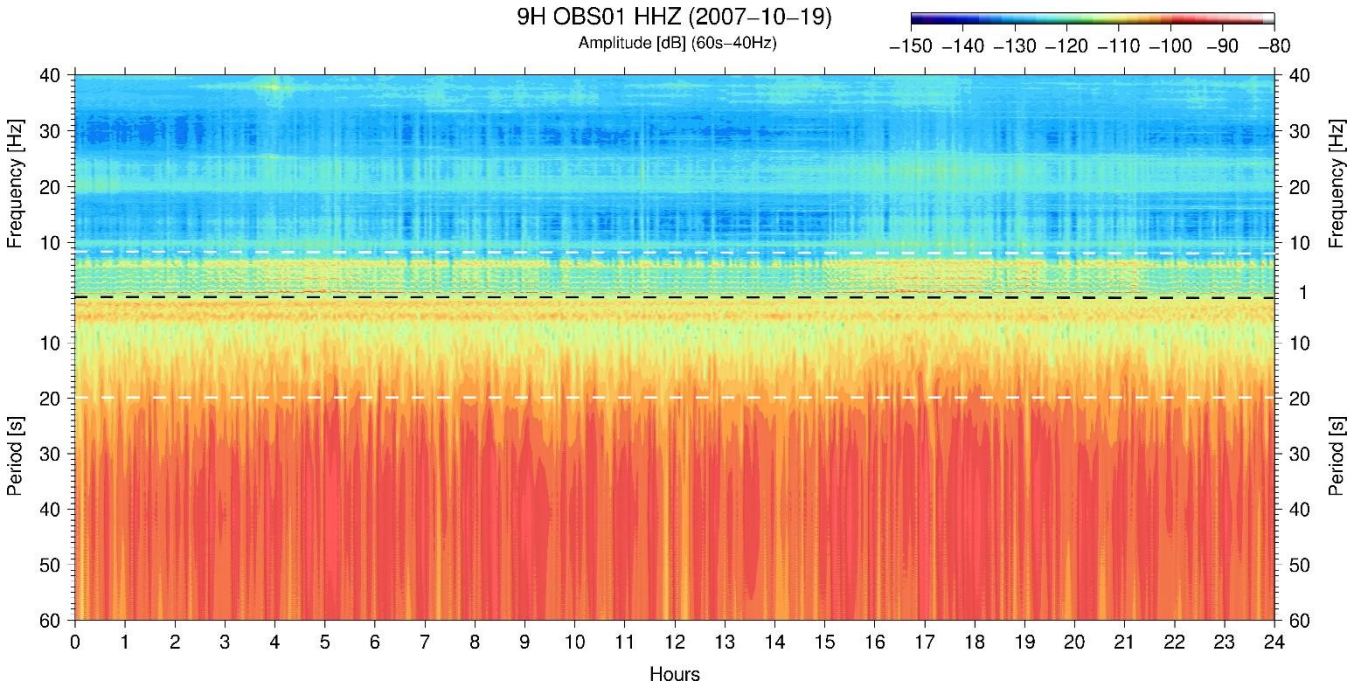
Data Resources

Supplemental material for this article includes a tide table from Lagos, Sines and Cascais and a spectrogram from 11 September 610 2007 (spring tide - new moon) to 28 September 2007 (spring tide -full moon). Figures for this article and supplemental material were created using Generic Mapping Tools (GMT) (Wessel et al., 2013) and ObsPy (Krischer et al., 2015). The LOBSTER OBS data, acquired in SW Iberia, near Portugal, is a contribution from project NEAREST FP6-2005-GLOBAL-4 (OJ 2005 C177/15). The new broadband OBS data were provided by DUNE project (PTDC/EAM-OCE/28389/2017) (<http://idl.campus.ciencias.ulisboa.pt/dune/>).

Acknowledgments

615 This article is a contribution of project NEAREST FP6-2005-GLOBAL-4 (OJ 2005 C177/15). Instruments were provided by “Deutscher Geräte-Pool für Amphibische Seismologie (DEPAS)” at Alfred Wegener Institute Bremerhaven and Deutsches Geoforschungszentrum Potsdam (<https://doi.org/10.17815/jlsrf-3-165>). The authors are also grateful to the crew of RV *Mário Ruivo* for the excellent support during deployment and retrieval of OBS on cruise EMSO-PT 2021. This work was funded by Portuguese Fundação para a Ciência e a Tecnologia (FCT) I.P./MCTES through national funds (PIDDAC) – 620 UIDB/50019/2020 -Instituto Dom Luiz (IDL).

Figures



625

Figure 1 | Noise bands – Inside the short-period band, from 0.5 to 6.5Hz, we show long-lasting harmonic tremors signals frequently observed in spectrograms of OBS data with overlapping frequency content with earthquake detection events (upper rectangle between white and black dashed line). The long-period band from 20s-60s shows the tilt noise (bottom rectangle) and the microseism noise band between 2s and 20s (middle rectangle between dashed lines). The harmonic tremors, microseism and tilt-noise are show in this particular OBS data records and 630 are continuously observed in one-day spectrogram (OBS01). The spectrogram is made between 40 Hz and 0.0167 Hz (60 seconds), however, between 1 Hz and 0.0167 Hz converted to period in seconds with linear axes. The amplitude unit is $\text{m}^2/\text{s}^4/\text{Hz}$ or dB.

635

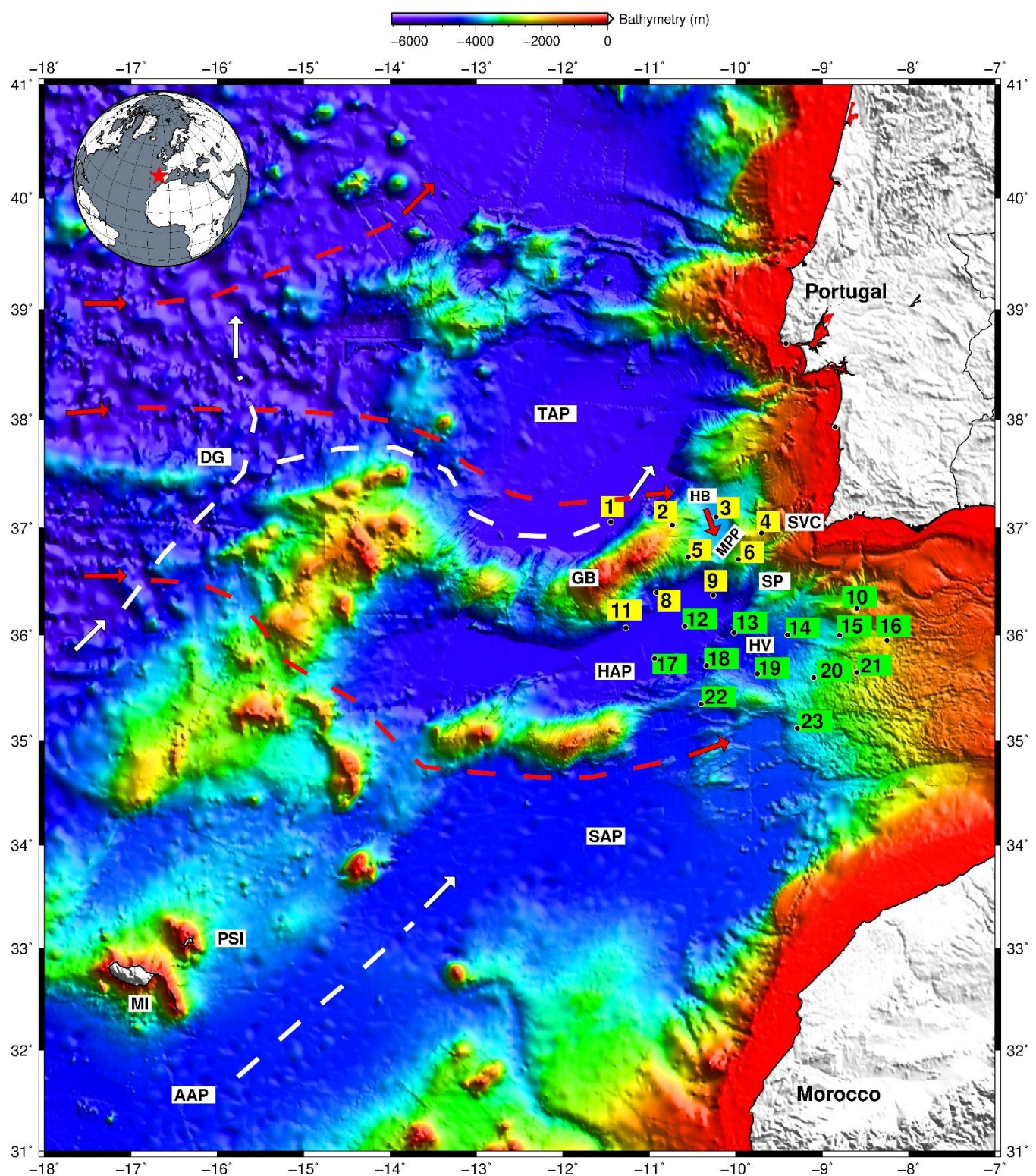


Figure 2 | LOBSTER OBS location - Deployment of OBS (1 represents OBS01, and so on). Main geographical features shown: TAP – Tagus Abyssal Plain; HB – D. Henrique Basin; DG – Discovery Gap; GB - Gorringe Bank; MPP – Marquês de Pombal Plateau; SVC – São Vicente Canyon; SP – Sagres Plateau; HAP – Horseshoe Abyssal Plain; SAP – Seine Abyssal Plain; AAP – Agadir Abyssal Plain; MI – Madeira Island; PSI – Porto Santo Island. The white dashed lines represent the Antarctic Bottom Water (AABW) flowing regionally below 4000 meters. The red dashed lines represent the North Atlantic Deep Water (NADW) flowing between 1400-4000 meters. We mark the OBSs that were affected or not by the ocean bottom current flow. Those affected are in yellow and those were not are in green. The OBS 9H OBS01, 9H OBS03 and 9H OBS04 are used in this study and the graphics are made with GMT (Wessel et al., 2013).

640

645

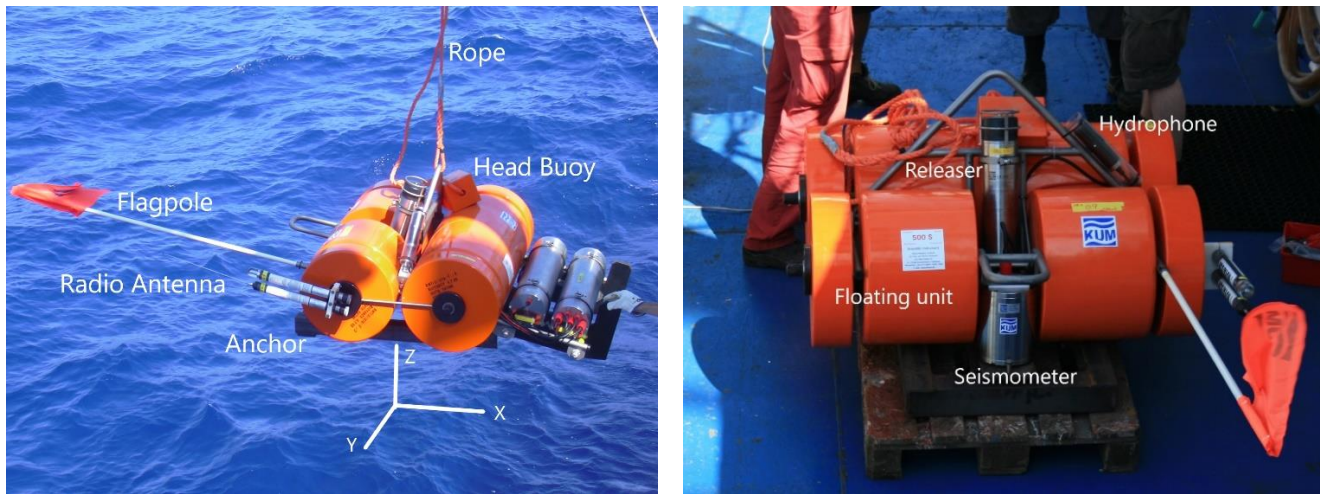
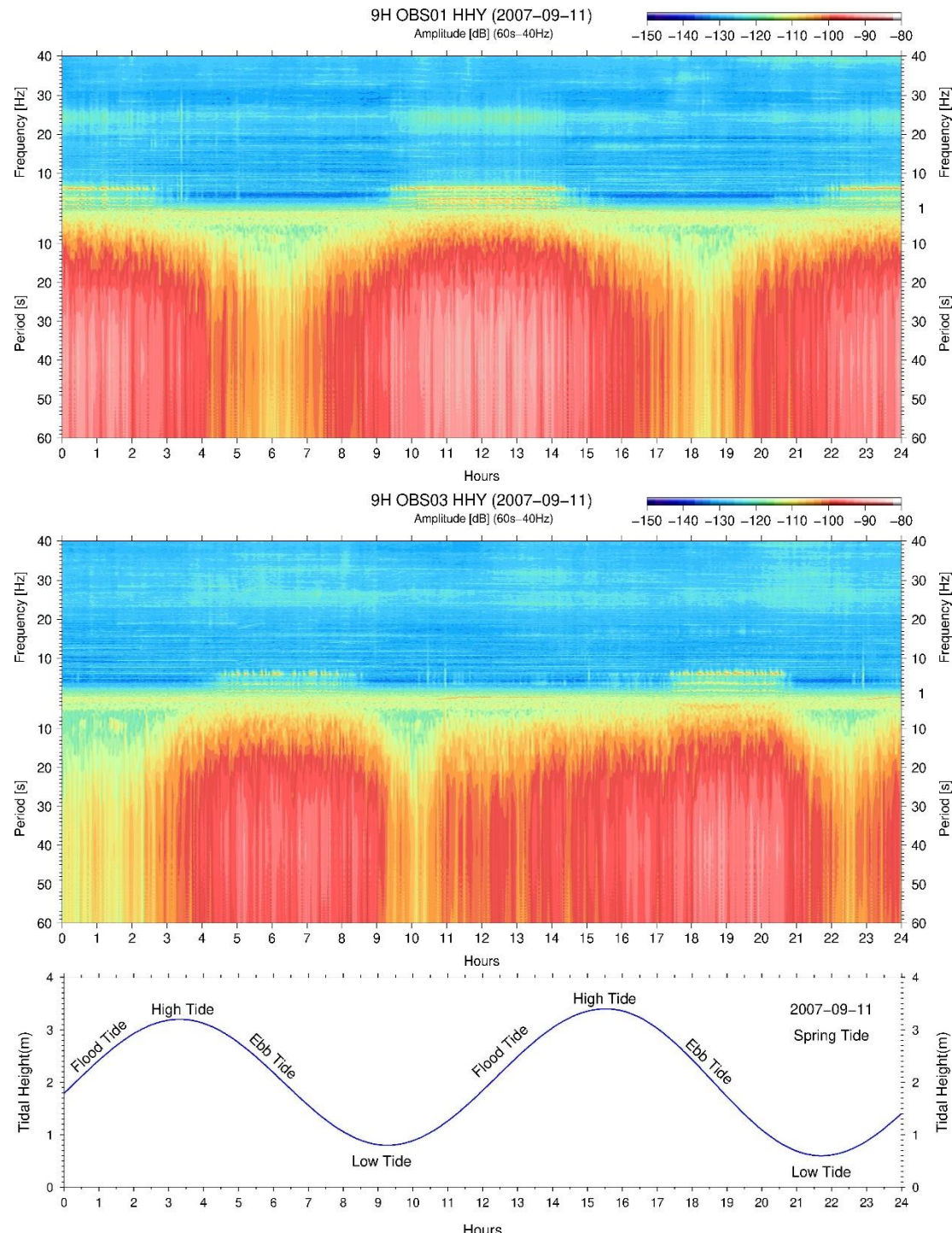


Figure 3 | LOBSTER OBS - Lobster OBS used in NEAREST project. On the left: OBS suspended by the ship's crane, waiting for the deploy signal. On the right: on deck ready to be deployed.



Figure 4 | DUNE OBS. New broadband OBS developed and build in Portugal with the new seismic sensor Aquarius (120s-100Hz) from GURALP and a broadband hydrophone HTI-04-PCA. On the left DUNE OBS on free-fall in the water column. On the right: Recovery of the DUNE OBS with the flag, radio and flashlight outside the orange shell. The deployment and recovery on board Portuguese vessel, RV *Mário Ruivo* (IPMA).

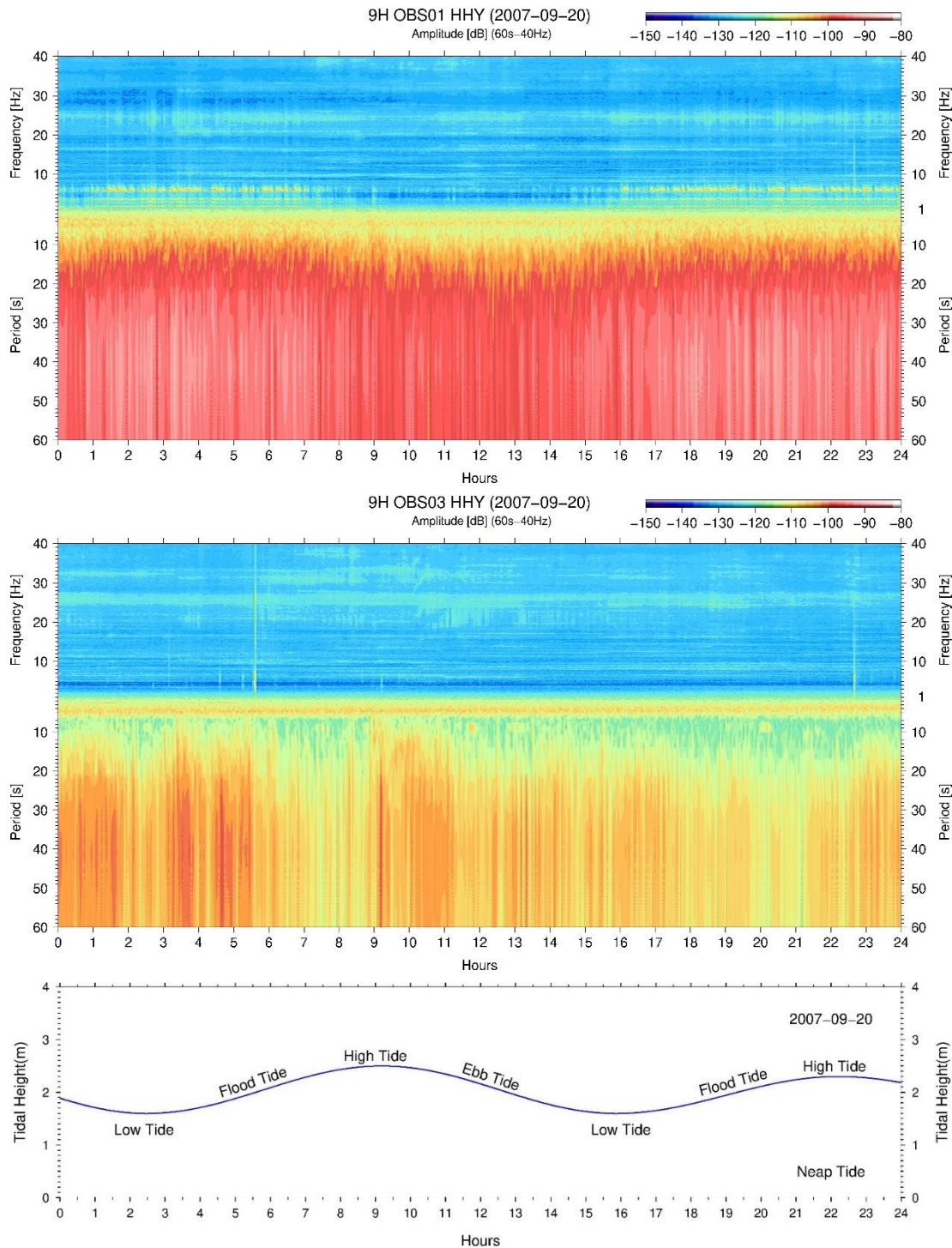


680 **Figure 5 | Spring Tide at new moon** – Spectrograms of 9H OBS01 and 9H OBS03 (11 September 2007) during the spring tide. The OBS shows different responds to the tide and low-frequency current flows. During the spring tide the tidal range in Sines was 2.8 meters.

685

690

695

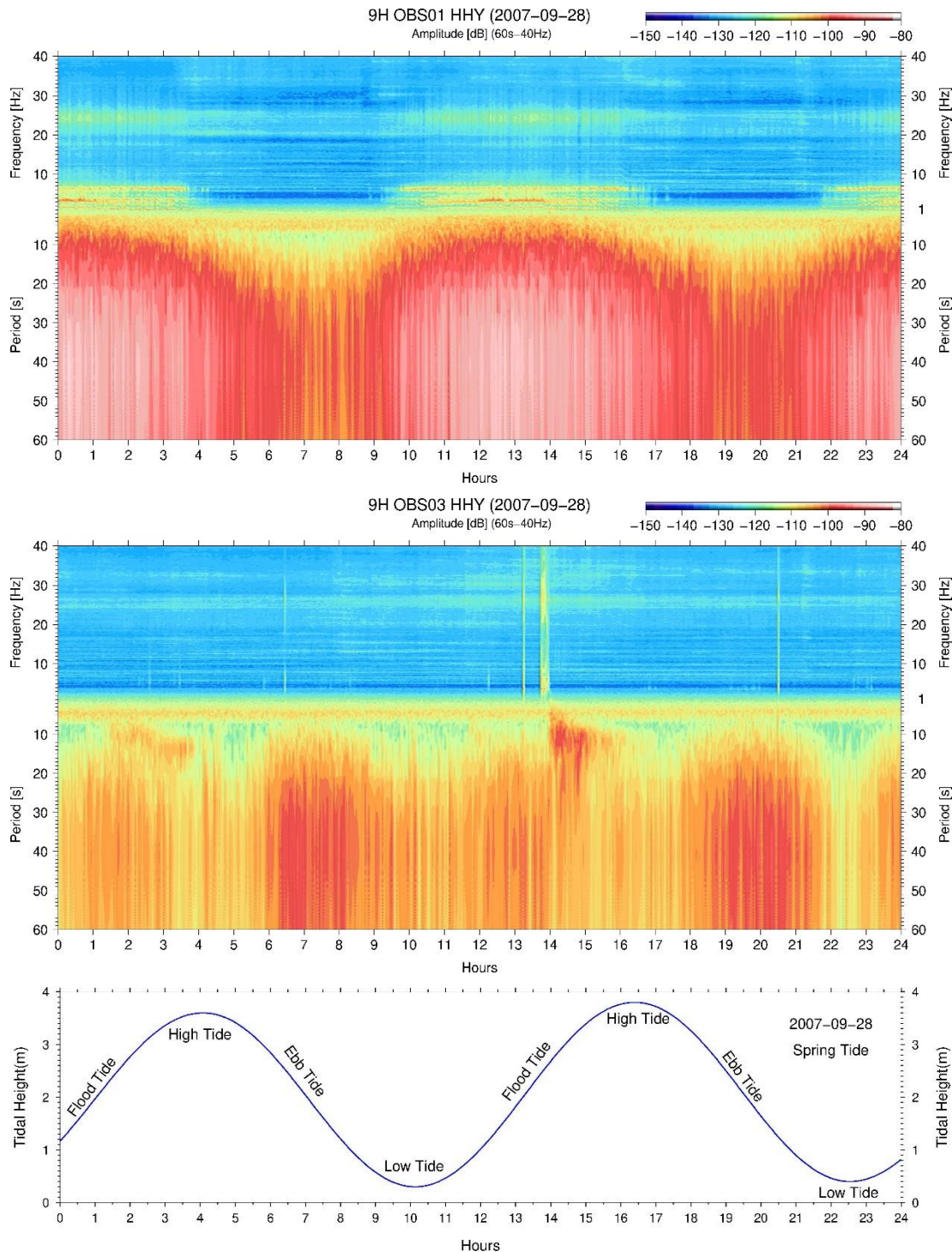


700 **Figure 6 | Neap tide in quarter moon – 9H OBS01 and 9H OBS03 spectrograms during the neap tide period (20 September 2007).** The permanent low-frequency flow dominates over the tide flow. The tidal range in neap tide was 0.7 meters (measured in Sines). In 9H OBS03 was observed the whale vocalization between 20 and 24Hz.

705

710

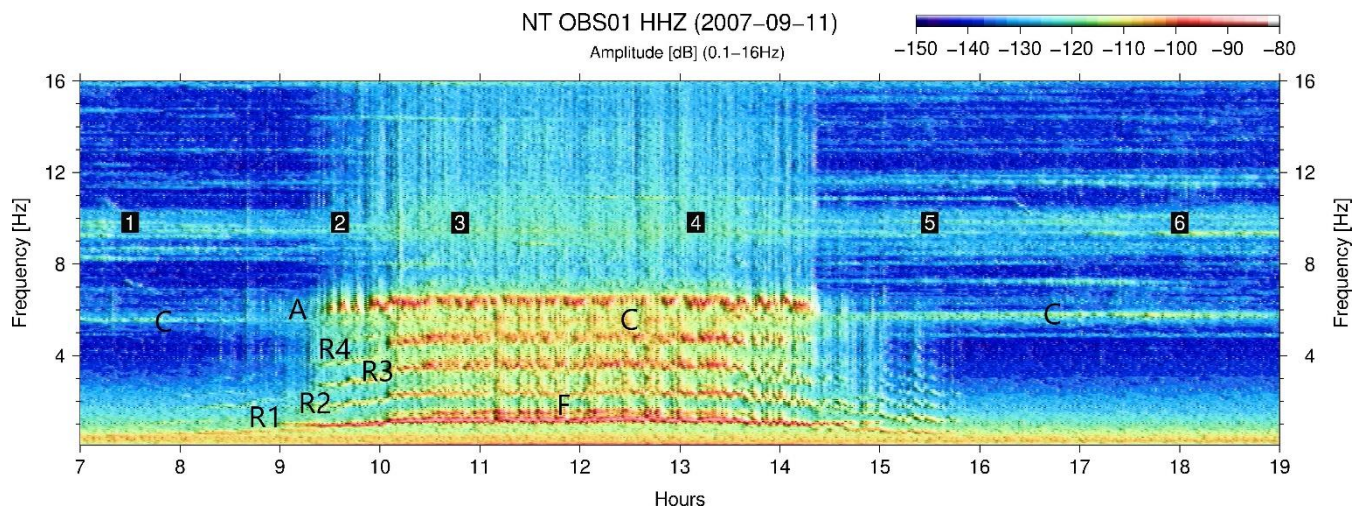
715



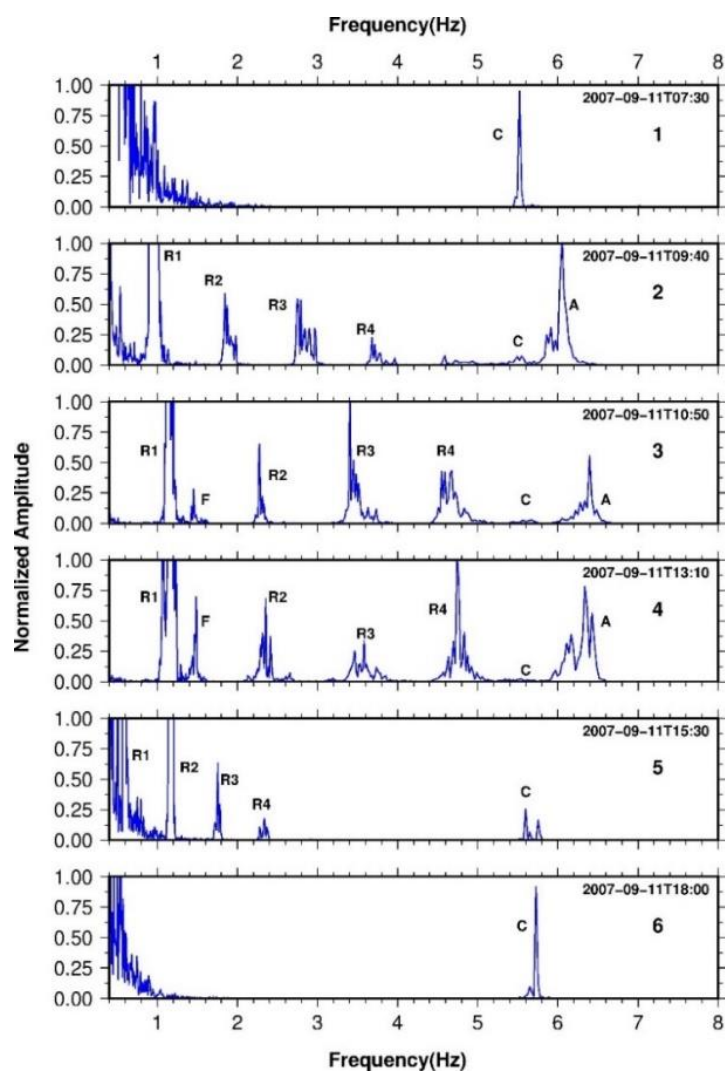
720 **Figure 7 | Spring Tide at full moon – 9H OBS01 and 9H OBS03 spectrograms during the spring tide (28 September 2007). The OBSs show different respond to the energy balance between tide and permanent low frequency flows. The 9H OBS01 during flood tide and 9H OBS03 in ebb tide. During the spring tide, the tidal range was 3.5 meters (measured in Sines).**

725

730



735



740

Figure 8 | Harmonic tremors— The prevailing signals before, during and after the harmonic tremors. The current flow speed describes in terms of (A) radio antenna, (F) flagpole, (R1) head buoy rope fundamental frequency, (R2) 2nd, (R3) 3rd, (R4) 4th overtones and (C) the natural frequency of OBS-sediments coupling. At (1) 07h30m, before the harmonic tremors, with his normal vibration; (2) 09h40m observed frequency gliding in the head buoy rope; (3) 10h50m we observe mode-locking frequency on harmonic tremor; (4) 13h10m continues the previous situation in terms of frequency (mode-locking); (5) 15h30 the current flow speed is decreasing and was observed a frequency-gliding of the head buoy rope; (6) 18h00m the harmonic tremor is no longer active and the natural frequency of OBS-sediments coupling return to normal.

745

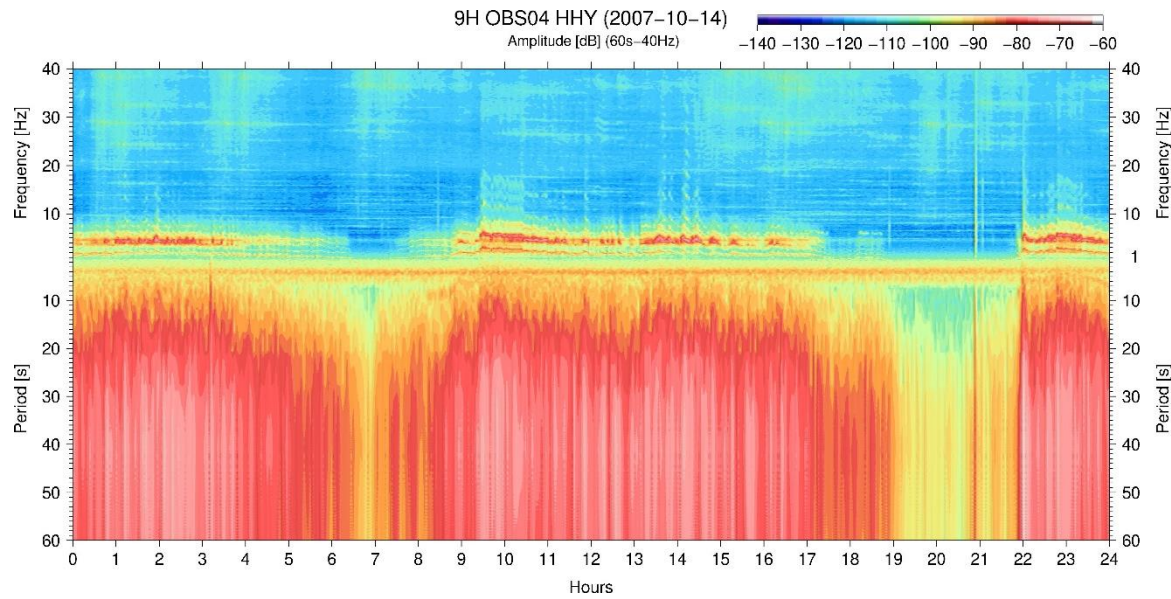


Figure 9 | Strong harmonic tremor. The effect of strong current flow speed when impacts the head buoy rope between 1-40Hz.

750

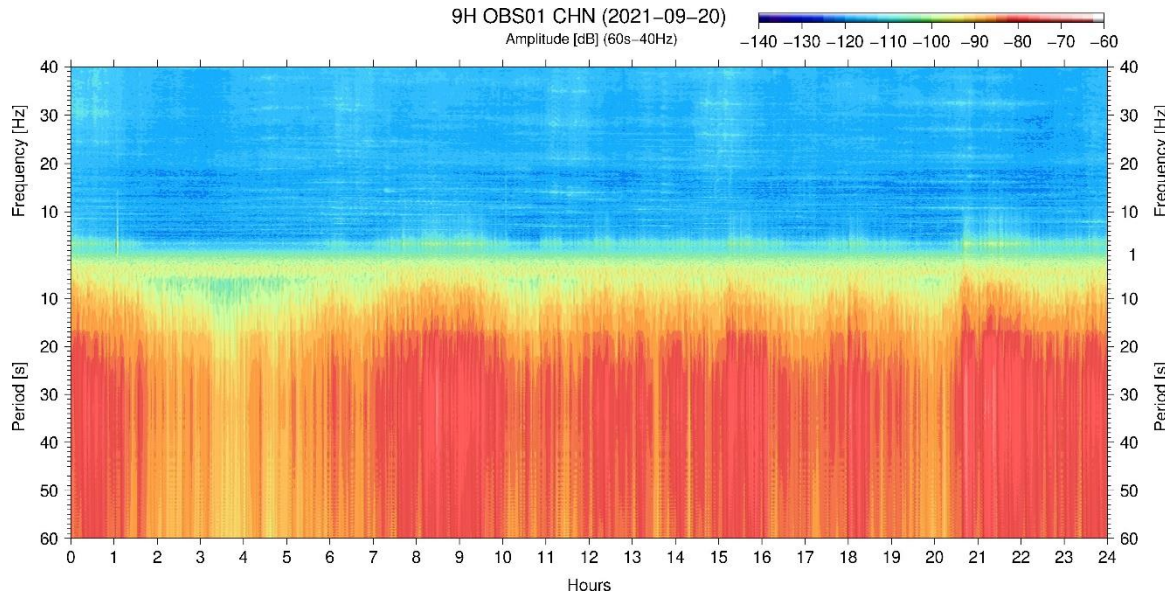
755

760

765

770

775



780

Figure 10 | LX OBS01 spectrogram. In this particular day a strong current flow scenario was observed during the campaign without harmonic tremors, however with noise around the natural frequency of OBS-sediment coupling resonance. The tilt noise, resulting from the current flow impact on the OBS structure, was observed almost during the entire day.

785

790

795

800

805

810

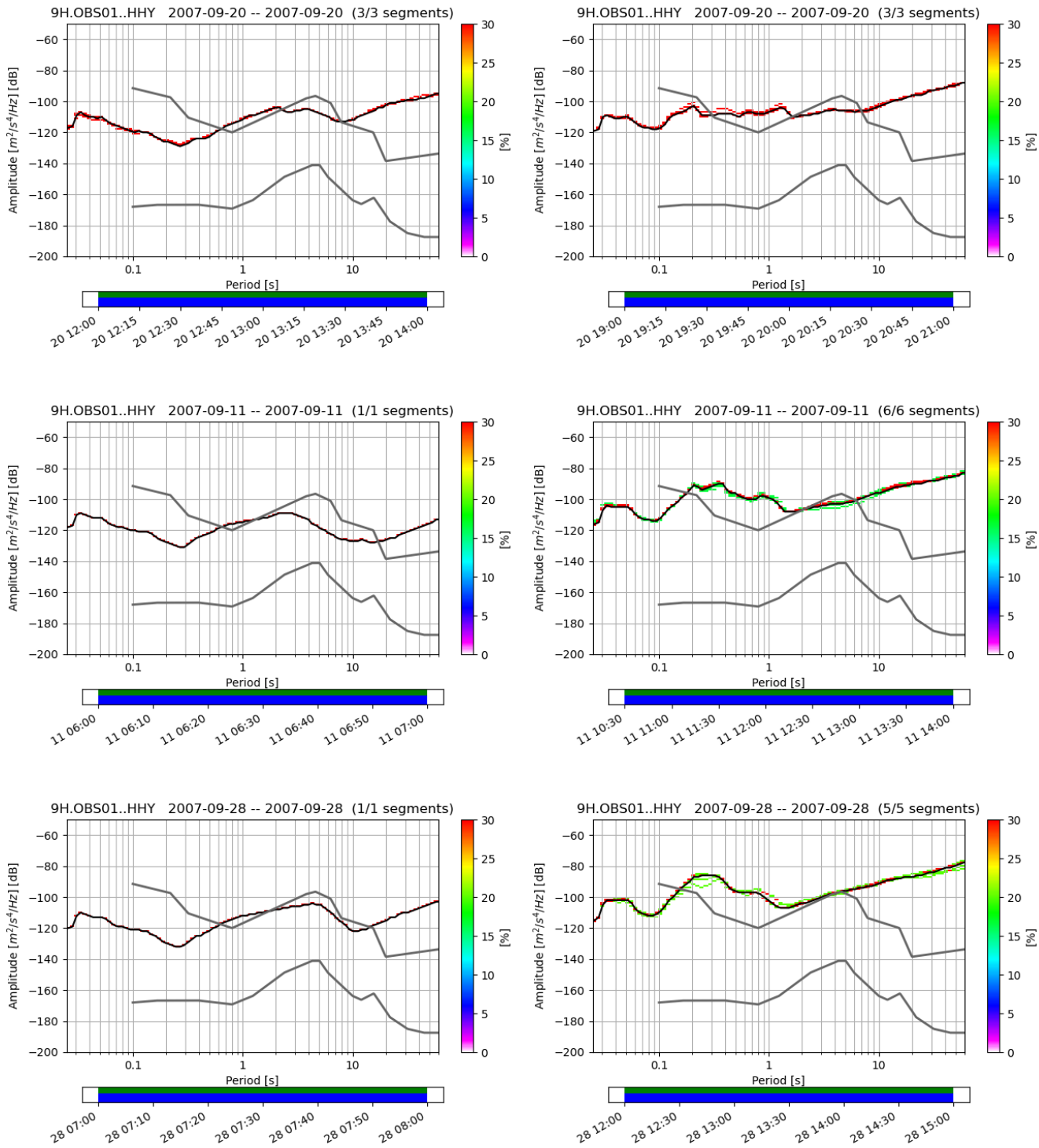


Figure 11 | PPSD of 9H OBS01 for the spring and neap tides – On top, PPSD for the 20 September 2007 (first quarter moon neap tide with 0.7m tidal range), middle at 11 September 2007 (new moon spring tide with 2.8m tidal range) and on the bottom the 27 September 2007 (full moon spring tide with 3.5m tidal range). On the left, seismometer response during laminar flow and on the right during turbulent flow.

815

820

825

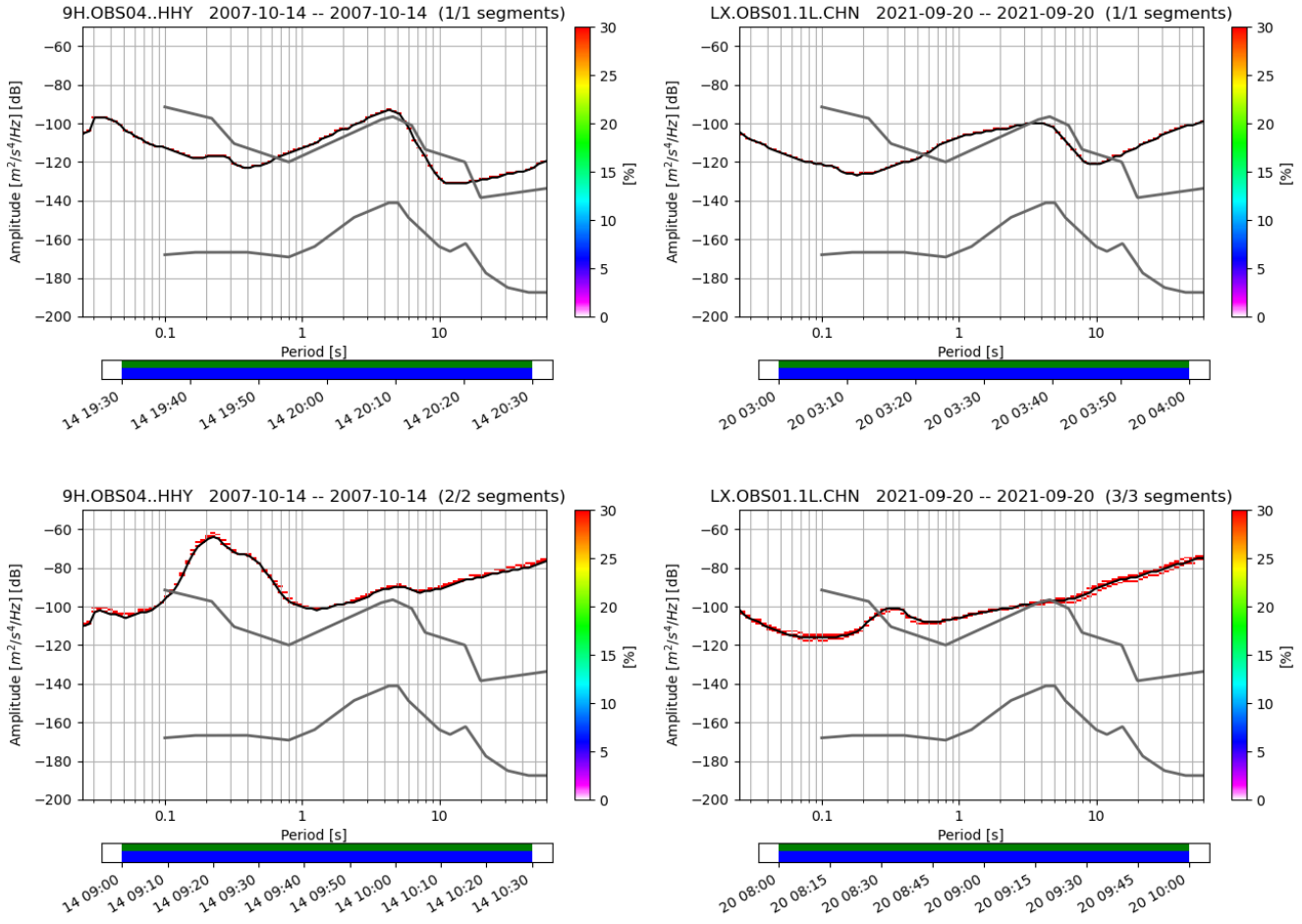


Figure 12 | PPSD of 9H OBS04 and LX OBS01 during laminar and turbulent flow events. Different high current flow speed scenario at 14 October 2007 (9H OBS04) and 20 of September 2021(LX OBS01). The upper part of the Figure represents the laminar flow scenario in both OBSs and the bottom part the turbulent one.

830

835

840

845

850

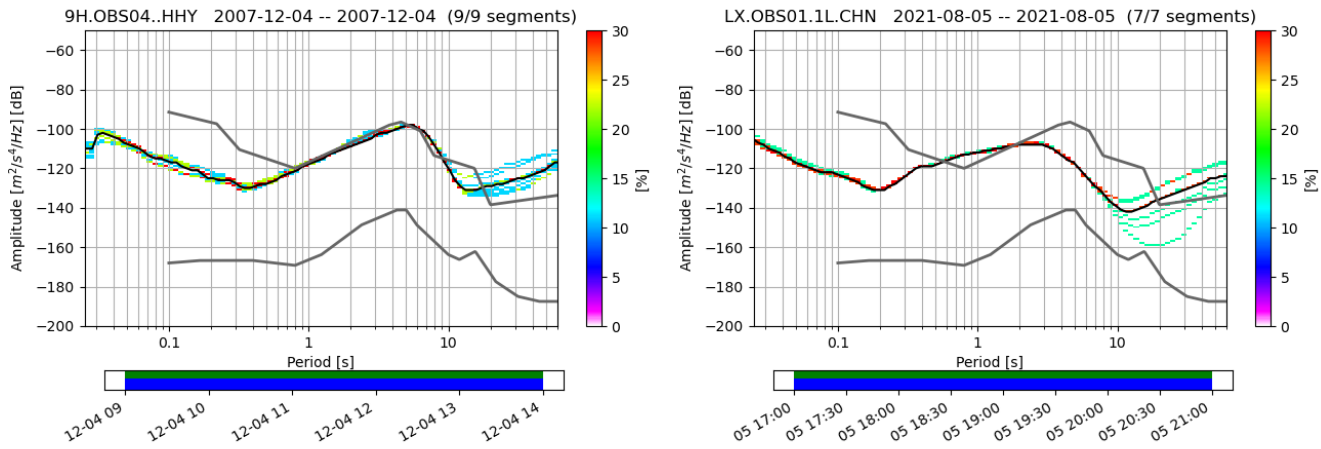


Figure 13 | Response – The response of CMG-40T and Aquarius seismometer, both from GURALP, to laminar flow.